Wideband Beam-forming Networks Utilizing Planar Hybrid Couplers and Phase Shifters

He Zhu, *Member, IEEE*, Maral Ansari, *Member, IEEE*, and Y. Jay Guo, *IEEE Fellow*

***Abstract*—In this paper, a new approach to designing 6 × 6 beam-forming networks for producing 5 or 6 beams is presented. The configuration of the 6 × 6 beam-forming networks is designed utilizing planar wideband hybrid couplers and phase shifters. A new type of wideband hybrid coupler is built based on a slotline resonator and microstrip-to-slotline transitions. The proposed coupler design can achieve high level of isolation between the sum and difference ports. Two different formats of wideband 6 × 6 beam-forming networks are then developed, to generate 5 and 6 beams, respectively. A prototype is fabricated and tested, and the experimental results agree with the simulation ones very well, achieving a wide operating bandwidth of more than 30%. Finally, the beam-forming network is verified by feeding a 6-element array, and the realized patterns match the predicted ones very well, demonstrating the function of the beam-forming network. The topology of an extended 12 × 12 beam-forming network is also given to demonstrate the possibility of creating higher order beam-forming networks using the presented approach.**

***Index Terms*—Beam-forming network, Butler matrix, hybrid coupler, microstrip, multi-beam, Nolen matrix, phase shifter, planar, slotline, wideband.**

I. Introduction

CIRCUIT-TYPE multi-beam antennas serve as a key technology for 5G and beyond wireless communication systems [1]. In order to obtain higher data capacities, multi-beam antenna arrays and multiple beam-forming networks (BFN) are widely investigated [2]-[4]. Typical multi-beam beam-formers include planar beam-forming networks, such as Blass matrices [5]-[6], Butler matrices (BM) [7]-[8], Nolen matrices [9]-[11], and lens antennas, such as Luneburg lens [12] and Rotman lens [13]. With the exception of the bulky Luneburg lens, most lens structures suffer from certain phase errors which limits the angular range and bandwidth of multibeams. Lens antennas are usually bulky and non-planar. Alternatively, passive multiple beam-forming networks can provide multiple beams with wide angular rangeat low cost.

Butler matrices are the most commonly used beam-formers in wireless communication systems, as they are planar, simple and non-dispersive in structure and can be lossless in principle. Butler matrices have been widely investigated for many years, and the most widely used fabrication technologies include printed circuit board (PCB) [14]-[15], substrate integrated waveguide (SIW) [16] and waveguides [17]. In comparison, PCB is the most widely used in current 4G LTE and 5G base stations where wide bandwidth is required. Conventional Butler matrices have 2^n input ports and 2^n output ports, typically in 4 × 4 format and 8 × 8 format. However, although such formats are simple, they may not be able to fulfill all the coverage requirements in many cases, especially when a flexible number of beams are required. In practice, supporting arbitrary number of beams would be more desirable where the number of beams is not constrained to 2^n. How to realize flexible number of beams was studied and a synthesis method was given in [18].

On the other hand, a Blass matrix and a Nolen matrix can be sized for use with any number of inputs and outputs. While the former has inherent low efficiency due to the resistive terminations, the latter is theoretically lossless, so it has attracted the attention of the research community recently. Although these structures are inherently dispersive due to their series-fed topology, modified topology of Nolen matrices to equalized the path length resulting in a broad frequency band operation similar to that of a Butler matrix are reported [19]-[21]. In [21], broadband Nolen matrix with a more "parallel" matrix topology in SIW technology is presented. a compact modified Nolen matrix topology generalized to one-dimensional and two-dimensional parallel switching matrices with an arbitrary number of beams was proposed in [22] and [23] recently.

One topology of multi-beam feed networks with flexible number of beams was proposed in [24], where applicable junctions other than hybrids are considered to increase the possible number of outputs. Many attempts have been made to produced three orthogonal beams including one in the boresight [25]-[29]. In [30]-[32], 3 × 4 format networks were studied to feed arrays with even number of elements. To extend the beam number, five or six orthogonal beams are realized in [33]-[35] and [36] using SIW and PCB technology, respectively. However, all of these designs have a narrow fractional bandwidth of around 5%, which is not suitable for the current prevalent 5G bands like Sub-6 GHz, and SIW is hard to be integrated with planar circuits in base stations. Research to further increase the bandwidth incorporating simple designs is in progress. In [37], a wideband coupler is presented and utilized in building a miniaturized Nolen matrix without using phase shifters.

Manuscript received November 10, 2021, revised April 8, 2022 and May 4, 2022, and accepted May 10, 2021.

The authors are with the Global Big Data Technologies Center (GBDTC), University of Technology Sydney, Ultimo, Sydney, NSW 2007, Australia. (email: he.zhu@uts.edu.au)

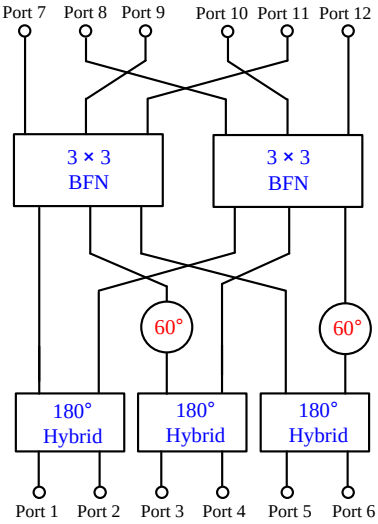

(a)

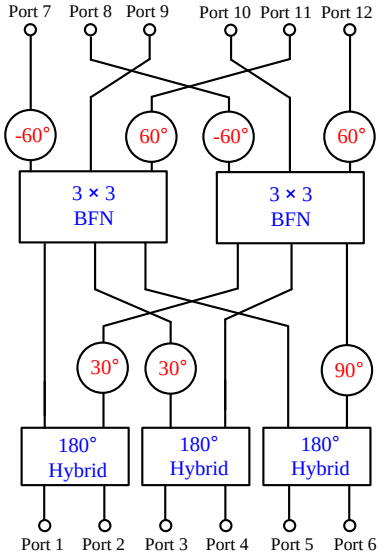

(b)

Fig. 1. Configurable of two types of 6 × 6 beam-forming networks: (a) 5-beam; (b) 6-beam.

TABLE I
Phase Increment Produced by 5- and 6-beam Beamforming Networks

5-Beam Beamforming Network						
Port number	1	2	3	4	5	6
Phase increment	0°	180°	-60°	120°	60°	-120°
6-Beam Beamforming Network						
Input port	1	2	3	4	5	6
Phase increment	30°	-150°	-30°	150°	90°	-90°

In this work, in order to achieve a wide operating bandwidth and obtain a flexible number of beams, we aim to develop wideband 6 × 6 beamforming networks (BFN) to produce 5 or 6 beams with at least 30% operation bandwidth. To this end, the synthesis of such BFN is given first, and then a new type of wideband hybrid coupler is proposed using planar structures. Based on the proposed couplers, two prototypes of planar 6 × 6 BFN are developed. The function of the 6 × 6 BFN is verified by feeding a linear antenna array, and multiple orthogonal beams with predictable radiation patterns are realized.

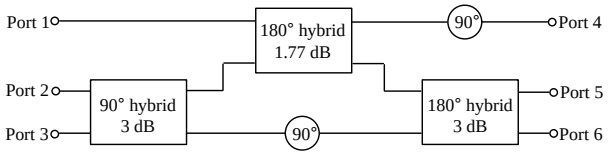

Fig. 2. Configuration of a 3 × 3 beam-forming network.

The contributions of the paper are as follows. First, we present a novel architecture of 6 × 6 beam-forming networks to produce 5 or 6 beams employing different configurations. Second, a thorough design procedure is given to guide how to realize non-conventional number of beams using such 6 × 6 BFN. Third, a new type of wideband hybrid couplers is built and implemented in 6 × 6 BFN using planar circuits. Finally, the topology of an extended 12 × 12 beam-forming network is given, demonstrating the possibility of upgrading the proposed beam-forming networks to higher orders using the presented design approach.

II. Synthesis of 5-beam and 6-beam Beamforming Networks

In this section, the configuration and working principles of 6 × 6 beamforming networks are presented. The proposed BFNs aim to realize a flexible number of beams in arrays. To this end, two beamforming networks with different topologies are given in Fig. 1(a) and (b), which can produce 5 and 6 beams, respectively. Table I shows all the phase increments produced by a 5-beam and 6-beam BFN, when different input ports are excited. The synthesis process of such beam-forming networks is given in the following part of this section.

A. 5-beam Beamforming Network

By observing Fig.1, one can find that the proposed 6 × 6 beamforming networks are composed of 180° hybrid couplers, 3 × 3 networks and phase shifters with different values. Fig. 2 shows the configuration of a typical 3 × 3 BFN. The phase increment at three output ports is 0°, -120° and 120°. It is composed of three hybrid couplers, including a 3-dB 90° coupler, a 3-dB 180° hybrid coupler (power division = 1:1) and a 1.77-dB 180° hybrid coupler (power division = 2:1). As the core component, the transmission matrices of the equal 90° hybrid coupler, 3-dB and 1.77-dB 180° hybrid couplers are expressed as:

$$[M]_{90^\circ HC} = \begin{bmatrix} \frac{1}{\sqrt{2}} & -j\frac{1}{\sqrt{2}} \\ -j\frac{1}{\sqrt{2}} & \frac{1}{\sqrt{2}} \end{bmatrix} \quad (1)$$

$$[M]_{180^\circ HC1} = \begin{bmatrix} \frac{1}{\sqrt{2}} & \frac{1}{\sqrt{2}} \\ \frac{1}{\sqrt{2}} & -\frac{1}{\sqrt{2}} \end{bmatrix} \quad (2)$$

$$[M]_{180^\circ HC2} = \begin{bmatrix} \frac{\sqrt{2}}{\sqrt{3}} & \frac{1}{\sqrt{3}} \\ \frac{1}{\sqrt{3}} & -\frac{\sqrt{2}}{\sqrt{3}} \end{bmatrix} \quad (3)$$

Besides, two 90° phase shifters are also used. For the 3 × 3 BFN, its transmission matrix can be expressed as:

$$[M]_{3\times3} = \begin{bmatrix} [M]_{90°\,HC} & \\ & 1 \end{bmatrix} \cdot \begin{bmatrix} j & \\ & [M]_{180°\,HC1} \end{bmatrix} \cdot \begin{bmatrix} [M]_{180°\,HC2} & \\ & j \end{bmatrix} = \frac{1}{\sqrt{3}} \begin{bmatrix} e^{-j\frac{\pi}{6}} & e^{-j\frac{5\pi}{6}} & e^{j\frac{\pi}{2}} \\ e^{-j\frac{\pi}{3}} & e^{j\frac{\pi}{3}} & -1 \\ 1 & 1 & 1 \end{bmatrix} \quad (4)$$

By performing elementary row transformation and neglecting the initial phase of the first element, the transmission matrix of a 3 × 3 BFN can be written in a simpler manner:

$$[M]'_{3\times3} = \frac{1}{\sqrt{3}} \begin{bmatrix} 1 & 1 & 1 \\ 1 & e^{-j\frac{2\pi}{3}} & e^{j\frac{2\pi}{3}} \\ 1 & e^{j\frac{2\pi}{3}} & e^{-j\frac{2\pi}{3}} \end{bmatrix} \quad (5)$$

Obviously, the phase difference between adjacent elements in each row is equal to 0, -120º and 120º, respectively, and it can be used as the fundamental matrix for building 6 × 6 BFN to realize six different phase increment values between elements, as shown in Fig. 1(a). It is composed of two 3 × 3 BFN, three 180° hybrid couplers and two 60° phase shifters. If no phase shifters are added after hybrid couplers, the phase increment of the 6 × 6 BFN would be 0º and 180º. When a phase shifter with phase shift value of φ is added, the phase increment at the outputs of the 6 × 6 BFN would become -φ and 180º-φ. Therefore, for the case of -60º and 120º, a phase shifter with 60º phase shift should be added after the first output port of the hybrid coupler; For the case of 60º and -120º, a phase shifter with 60º phase shift should be added after the second output port of the hybrid coupler. The transmission matrix of the 6 × 6 BFN can be expressed as:

$$[M]_{6\times6} = \frac{1}{\sqrt{2}} \begin{bmatrix} 1 & & & 1 & & \\ & e^{j\frac{\pi}{3}} & & & 1 & \\ & & 1 & & & e^{j\frac{\pi}{3}} \\ 1 & & & -1 & & \\ & e^{j\frac{\pi}{3}} & & & -1 & \\ & & 1 & & & -e^{j\frac{\pi}{3}} \end{bmatrix} \cdot \begin{bmatrix} [M]'_{3\times3} & \\ & [M]'_{3\times3} \end{bmatrix}$$

$$= \frac{1}{\sqrt{6}} \begin{bmatrix} 1 & 1 & 1 & 1 & 1 & 1 \\ e^{j\frac{\pi}{3}} & e^{-j\frac{\pi}{3}} & e^{j\pi} & 1 & e^{-j\frac{2\pi}{3}} & e^{j\frac{2\pi}{3}} \\ 1 & e^{j\frac{2\pi}{3}} & e^{-j\frac{2\pi}{3}} & e^{j\frac{\pi}{3}} & e^{j\pi} & e^{-j\frac{\pi}{3}} \\ 1 & 1 & 1 & -1 & -1 & -1 \\ e^{j\frac{\pi}{3}} & e^{-j\frac{\pi}{3}} & e^{j\pi} & -1 & e^{j\frac{\pi}{3}} & e^{-j\frac{\pi}{3}} \\ 1 & e^{j\frac{2\pi}{3}} & e^{-j\frac{2\pi}{3}} & e^{-j\frac{2\pi}{3}} & 1 & e^{j\frac{2\pi}{3}} \end{bmatrix} \quad (6)$$

Considering the crossovers at the outputs, elementary column transformations need to be done in $[M]_{6\times6}$, which means that it has the same function with the following matrix:

$$[M]'_{6\times6} = \frac{1}{\sqrt{6}} \begin{bmatrix} 1 & 1 & 1 & 1 & 1 & 1 \\ e^{j\frac{\pi}{3}} & 1 & e^{-j\frac{\pi}{3}} & e^{-j\frac{2\pi}{3}} & -1 & e^{j\frac{2\pi}{3}} \\ 1 & e^{j\frac{\pi}{3}} & e^{j\frac{2\pi}{3}} & -1 & e^{-j\frac{2\pi}{3}} & e^{-j\frac{\pi}{3}} \\ 1 & -1 & 1 & -1 & 1 & -1 \\ e^{j\frac{\pi}{3}} & -1 & e^{-j\frac{\pi}{3}} & e^{j\frac{\pi}{3}} & -1 & e^{-j\frac{\pi}{3}} \\ 1 & e^{-j\frac{2\pi}{3}} & e^{j\frac{2\pi}{3}} & 1 & e^{-j\frac{2\pi}{3}} & e^{j\frac{2\pi}{3}} \end{bmatrix} \quad (7)$$

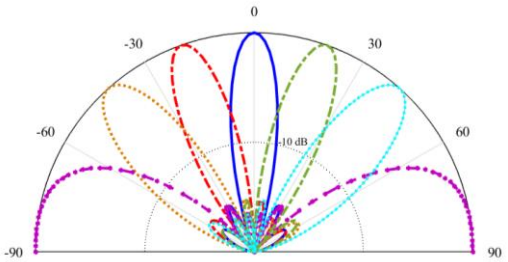

Fig. 3. Radiation patterns produced by a 5-beam BFN.

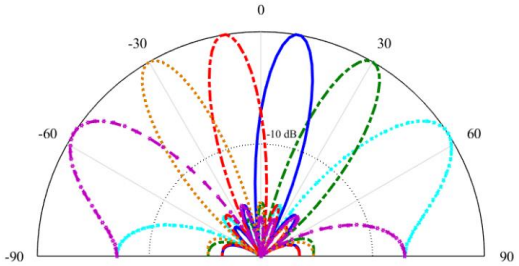

Fig. 4. Radiation patterns produced by a 6-beam BFN.

It is observed from (7) that the phase increment between adjacent elements in each row is equal to 0°, -60°, 60°, 180°, 120°, and -120°, respectively. When feeding a linear array using multiple excitations with equal magnitude and these phase increments, six different patterns can be realized. Fig. 3 displays the synthesized patterns which are produced by feeding a 6-element linear array with half-wavelength spacing using the excitations with phase increments listed in $[M]'_{6\times6}$. It is noted that when the phase increment is 180°, the realized pattern will be a differential pattern with two maximum gain points radiating towards two opposite directions. However, such kind of split-beam patterns are not useful in wireless communication systems. Therefore, this 6×6 BFN can produce five useful beams including two radiating towards left side, two towards right side and one at boresight, and one differential beam, indicating that it is a 5-beam BFN.

B. Modified 6-beam Beamforming Network

To make full use of a 6 × 6 BFN, we aim to avoid this differential pattern (produced by 180º phase increment) and convert it to a useful beam by using a modified 6 × 6 BFN. The configuration of the modified BFN is given in Fig. 1(b). This modified 6 × 6 BFN has the same number of 3 × 3 BFN and 180° hybrid couplers and more numbers of phase shifters compared with the first design. For the case of 30º and -150º, a phase shifter with 30º phase shift should be added after the second output port of the hybrid coupler. For the case of -30º and 150º, a phase shifter with 30º phase shift should be added after the first output port of the hybrid coupler. For the case of 90º and -90º, a phase shifter with 90º phase shift should be added after the second output port of the hybrid coupler. Besides, two additional pairs of phase shifters with -60º and 60º phase shift are needed at the outputs of the BFN to make the phase increment continuous. As a result, the transmission matrix of the modified 6 × 6 BFN can be expressed as:

$$[M]_{6\times6}^{modi} = \frac{1}{\sqrt{2}}\begin{bmatrix} 1 & & & e^{j\frac{\pi}{6}} & & \\ & e^{j\frac{\pi}{6}} & & & 1 & \\ & & 1 & & & e^{j\frac{\pi}{2}} \\ 1 & & & -e^{j\frac{\pi}{6}} & & \\ & e^{j\frac{\pi}{6}} & & & -1 & \\ & & 1 & & & -e^{j\frac{\pi}{2}} \end{bmatrix} \cdot \begin{bmatrix} [M]'_{3\times3} & \\ & [M]'_{3\times3} \end{bmatrix} \cdot \begin{bmatrix} [M]_{PS} & \\ & [M]_{PS} \end{bmatrix} \quad (8)$$

where

$$[M]_{PS} = \begin{bmatrix} -e^{j\frac{\pi}{3}} & & \\ & 1 & \\ & & e^{j\frac{\pi}{3}} \end{bmatrix} \quad (9)$$

Therefore,

$$[M]_{6\times6}^{modi} = \frac{1}{\sqrt{6}}\begin{bmatrix} e^{-j\frac{\pi}{3}} & 1 & e^{j\frac{\pi}{3}} & e^{-j\frac{\pi}{6}} & e^{j\frac{\pi}{6}} & e^{j\frac{\pi}{2}} \\ e^{-j\frac{\pi}{6}} & e^{-j\frac{\pi}{2}} & e^{-j\frac{5\pi}{6}} & e^{-j\frac{\pi}{3}} & e^{-j\frac{2\pi}{3}} & -1 \\ e^{-j\frac{\pi}{3}} & e^{j\frac{2\pi}{3}} & e^{-j\frac{\pi}{3}} & e^{j\frac{\pi}{6}} & e^{-j\frac{5\pi}{6}} & e^{j\frac{\pi}{6}} \\ e^{-j\frac{\pi}{3}} & 1 & e^{j\frac{\pi}{3}} & e^{j\frac{5\pi}{6}} & e^{-j\frac{5\pi}{6}} & e^{-j\frac{\pi}{2}} \\ e^{-j\frac{\pi}{6}} & e^{-j\frac{\pi}{2}} & e^{-j\frac{5\pi}{6}} & e^{j\frac{2\pi}{3}} & e^{j\frac{\pi}{3}} & 1 \\ e^{-j\frac{\pi}{3}} & e^{j\frac{2\pi}{3}} & e^{-j\frac{\pi}{3}} & e^{-j\frac{5\pi}{6}} & e^{j\frac{\pi}{6}} & e^{-j\frac{5\pi}{6}} \end{bmatrix} \quad (10)$$

To reduce the number of crossovers at the output ports, elementary column transformations are performed on $[M]_{6\times6}^{modi}$ and the final transmission matrix of the modified 6-beam BFN is transformed to be:

$$[M]_{6\times6}^{modi'} = \frac{1}{\sqrt{6}}\begin{bmatrix} e^{-j\frac{\pi}{3}} & e^{-j\frac{\pi}{6}} & 1 & e^{j\frac{\pi}{6}} & e^{j\frac{\pi}{3}} & e^{j\frac{\pi}{2}} \\ e^{-j\frac{\pi}{6}} & e^{-j\frac{\pi}{3}} & e^{-j\frac{\pi}{2}} & e^{-j\frac{2\pi}{3}} & e^{-j\frac{5\pi}{6}} & -1 \\ e^{-j\frac{\pi}{3}} & e^{j\frac{\pi}{6}} & e^{j\frac{2\pi}{3}} & e^{-j\frac{5\pi}{6}} & e^{-j\frac{\pi}{3}} & e^{j\frac{\pi}{6}} \\ e^{-j\frac{\pi}{3}} & e^{j\frac{5\pi}{6}} & 1 & e^{-j\frac{5\pi}{6}} & e^{j\frac{\pi}{3}} & e^{-j\frac{\pi}{2}} \\ e^{-j\frac{\pi}{6}} & e^{j\frac{2\pi}{3}} & e^{-j\frac{\pi}{2}} & e^{j\frac{\pi}{3}} & e^{-j\frac{5\pi}{6}} & 1 \\ e^{-j\frac{\pi}{3}} & e^{-j\frac{5\pi}{6}} & e^{j\frac{2\pi}{3}} & e^{j\frac{\pi}{6}} & e^{-j\frac{\pi}{3}} & e^{-j\frac{5\pi}{6}} \end{bmatrix} \quad (11)$$

It is observed from (11) that the phase increments between any two adjacent elements in each row is equal to 30°, -30°, 90°, -150°, 150°, and -90°, respectively. When feeding a linear array using multiple excitations with equal power and these phase increments, six different patterns can be realized, including three beams radiate towards left side and three towards right side, as displayed in Fig. 4. It is found that the modified 6 × 6 BFN has converted the split pattern to a useful beam successfully, extending the number of beams from 5 to 6, providing more flexibility when choosing the beam number.

III. Planar Structure Implementation

To implement the proposed 6 × 6 BFNs in the RF domain, PCBs are used for circuit development. As the key component of the BFNs, a new type of 180º hybrid coupler with wide operating bandwidth and high isolation is designed. According to the design objectives, it is required that the proposed coupler should have more than 30% operating bandwidth, and the power division at output ports should be 1:1 and 2:1. Based on such design, a 3 × 3 BFNs is built first, and based on this design, then extended to 6 × 6 ones. The rest part of this section describes such hybrid coupler and a planar 3 × 3 BFN design.

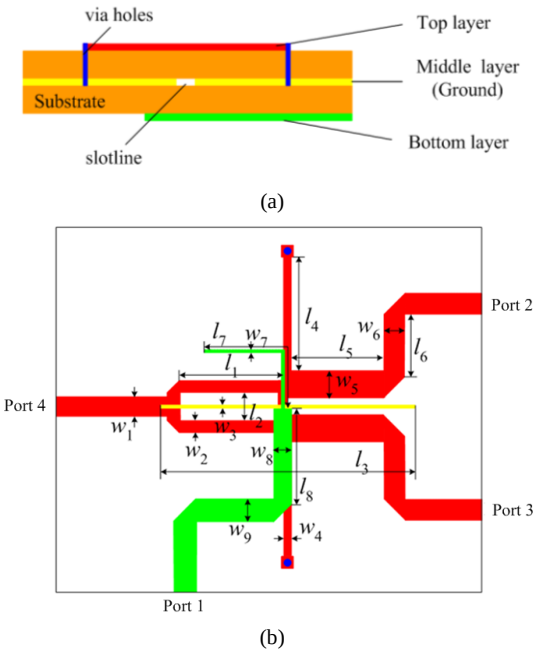

Fig. 5. Layout of the proposed wideband hybrid coupler: (a) sideview (from port 1); (b) top-view with dimensions.

A. Design of 180º Hybrid Couplers

By studying the literature, one can find that most of existing designs, such as traditional rat-race ring structures suffer from narrow bandwidth or unsatisfactory isolation. To overcome these problems, this section will present a new design of wideband hybrid coupler with ultra-high isolation and wide bandwidth. The proposed hybrid coupler is based on a multi-layer structure comprising three metal layers and two substrate layers, as displayed in Fig. 5(a). The top and bottom metal layers use microstrip lines, while the middle metal layer serves as the ground with a slotline on it. The adopted substrate has a dielectric constant of 3.48 and thickness of 0.76 mm.

Fig. 5(b) shows the top view of the design describing the layout information of all three metal layers. The red and green parts represent the microstrip lines on the top and bottom layer, and the yellow line refers to the slotline in the middle ground. Ports 1 and 4 function as the Δ port and Σ port, while ports 2 and 3 are the outputs. The short-ended stubs and transmission lines connecting port 2 and 3 form an L-shaped network, which will introduce multiple resonances and form a wide passband.

When port 1 is excited, the input signals will be split equally in magnitude at port 2 and 3 but with 180° phase difference between two output signals. It is noted that the signals excited at port 1 is coupled from the bottom layer to the slotline in the middle ground, and then flow to the outputs on the top layer. The transition occurs at the middle point of the slotline, where a narrow open-ended stub is perpencularly placed forming a microstrip-to-slotline transition [38][39]. This transition helps with transmit signals from bottom layer to top layer and vice

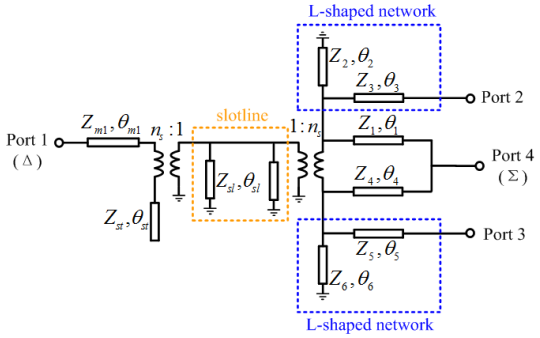

Fig. 6. Equivalent transmission line circuit of the hybrid coupler.

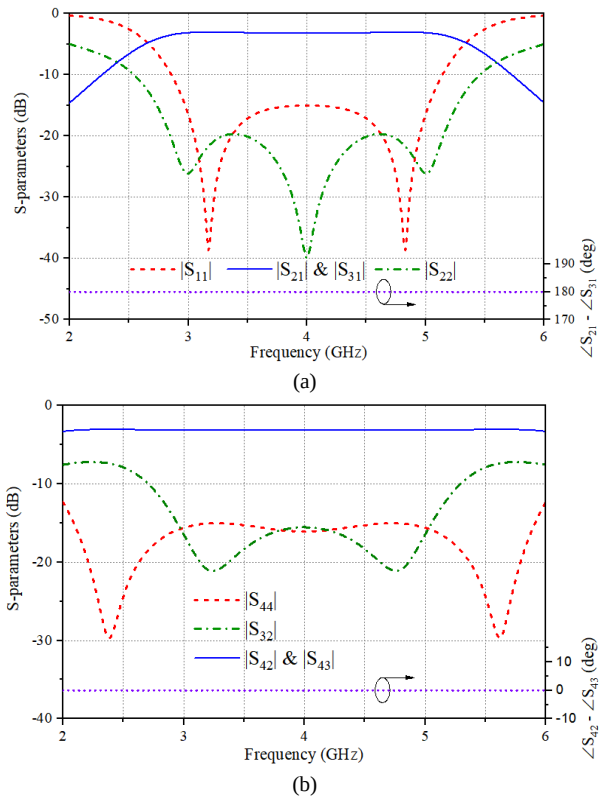

Fig. 7. Synthesized S-parameters of a 3-dB and 1.77-dB hybrid couplers.

versa. This is because the field distribution produced by the injected current from port 1 is in line with that of the slotline, which prompts the signals coupled into the slotline via magnetic coupling [39]. The field distribution in the slotline also accounts for the phenomenon of equal power and out-of-phase characteristics at outputs. On the other hand, when port 4 is excited, the input signals will be split equally with identical magnitude and phase at port 2 and 3. Due to the orthogonal distribution of electrical fields in the slotline and microstrip at the transition point, the isolation between port 1 and 4 is infinite in theory.

The proposed design can be analyzed using an equivalent transmission line circuit, which can predict its performance by synthesizing the scattering matrix of such four-port network. Fig. 4 shows the equivalent transmission line circuit of the design, which comprises of two transformers, two quarter-wavelength arms two L-shaped networks, two short-ended stubs representing the slotline, an open-ended stub and an impedance transformer at port 1. To obtain a wide bandwidth

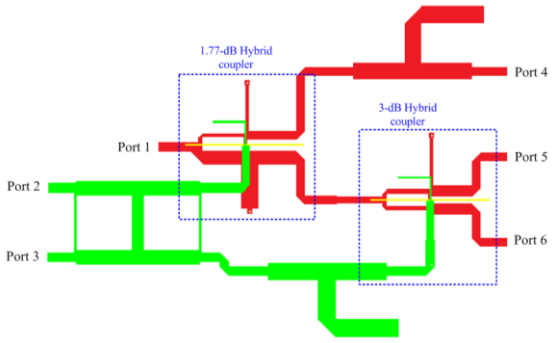

Fig. 8. Layout of a wideband 3 × 3 BFN.

and symmetrical response along the center frequency, all the stubs and transmission lines should be selected as λ/4.

To make all ports perfectly matched to Z_o, there should be $Z_1^2 \cdot Z_o = 2Z_3^2 \cdot Z_o$, and thus $Z_1 = \sqrt{2}Z_3$. When either the Σ- or Δ-port is excited, three resonances can be realized to form a wide operating band, resulting in a wide operating bandwidth of the hybrid coupler. Port 1 and port 4 are perfectly isolated because when port 1 is excited, port 4 can be regarded as open-circuit, and hence no current is coupled into the slotline and bottom layer. On the other hand, when port 4 is excited, port 1 can be regarded as a virtual ground and short-circuit, and thus no current would flow into port 1.

Fig. 7 shows the synthesized results of the equivalent circuit. The center frequency is set to be 4 GHz. The transmission coefficient of S_{21}, S_{31}, S_{24} and S_{34} is equal to -3 dB from 3 GHz to 5 GHz. Wideband matching performance at all ports (S_{11}, S_{22}, S_{33} and S_{44}) and high isolation between outputs (S_{32}) are achieved. The isolation between port Σ and Δ (S_{41}) is equal to 0 at all frequencies, indicating extremely high isolation of the design. It is also noted that the phase difference of $\angle S_{21} - \angle S_{31}$ and $\angle S_{42} - \angle S_{32}$ is 180° and 0° in a wideband range, respectively.

B. Wideband 3 × 3 Beamforming Network

To build a 6 × 6 BFN, the first step is to have a wideband 3 × 3 BFN, which could be realized using the proposed 180° hybrid coupler. As indicated in Fig. 1, one equal 3-dB hybrid coupler and one unequal 1.77-dB hybrid coupler are needed. The output power at port 2 and port 3 are determined by the impedance of two arms connected with port 1, which are $\sqrt{(1+k^2)} \cdot Z_o/k^2$, and $\sqrt{(1+k^2)} \cdot Z_o$, and k^2 refers to the power ratio between port 2 and port 3. For 3-dB couplers, $k^2 = 1$, and thus the impedance of two arms is $\sqrt{2}Z_o$. For 1,77-dB couplers, $k^2 = 2$, and thus the impedance of two arms is $\sqrt{3}Z_o/2$ and $\sqrt{3}Z_o$, respectively. Fig. 8 shows the layout of a wideband 3 × 3 BFN. A two-section branch-line coupler is used as the 3-dB 90° coupler. For the 90° phase shifters, the open-stub-loaded T-shaped phase shifter is adopted, which was introduced in [29], for it has a wide operation bandwidth. The T-shaped phase shifter uses two quarter-wavelengths transmission lines and a half-wavelength open-ended stub, by changing its impedance one can control the deviation of the phase shift. In Fig. 8, when port 1, 2 or 3 is excited, the theoretical phase increment between port 4, 5 and 6 is 0°, 120° and -120°, respectively.

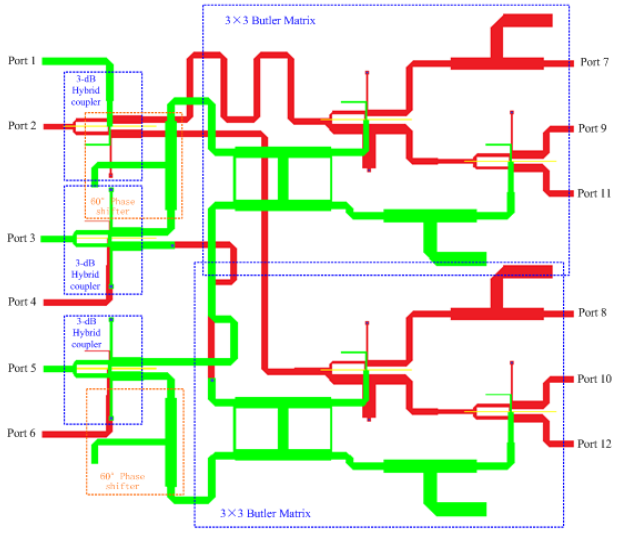

Fig. 9. Layout of the proposed 5-beam BFN.

To verify the performance of the 3 × 3 BFN, an EM model is built and full-wave simulation is done in the electromagnetic environment of Ansys' High-Frequency Structure Simulator (HFSS). The dimensions of hybrid couplers are: $l_1 = 8.4$, $l_2 = 2.4$, $l_3 = 18.2$, $l_4 = 9.5$, $l_5 = 8.7$, $l_6 = 5.4$, $l_7 = 9.2$, $l_8 = 9.4$, $l_8 = 21.8$, $w_1 = 2.1$, $w_2 = 0.8$, $w_3 = 0.3$, $w_4 = 0.6$, $w_5 = 3.6$, $w_6 = 1.7$, $w_7 = 0.4$, $w_8 = 1.3$, $w_9 = 1.7$, all in mm. The objective operating band range is from 3.25 GHz to 4.75 GHz (FBW is 37.5%). For brevity, the full-wave simulation results are not given here. When port 1, 2 or 3 is excited, the phase difference of $\angle S_{5i} - \angle S_{4i}$ and $\angle S_{6i} - \angle S_{5i}$ (i = 1, 2 or 3) is around 0°, 120° and -120° with the deviation of ±5°, which indicates excellent linearity in a wideband range and is favored for developing larger-scale beam-forming networks.

IV. Implementation of 6 × 6 Beamforming Networks and Experimental Verification

A. *Implementation of 6 × 6 Beamforming Networks*

In this section, a 5-beam and a modified 6-beam 6 × 6 BFN will be implemented using planar PCB technology. According to Fig. 1, the 6 × 6 BFN are composed of two 3 × 3 BFN, three hybrid couplers and two phase shifters, which are all introduced in the last section. For EM implementation, the same layer configuration shown in Fig. 5(a) is utilized. The layout of the 5-beam BFN for full-wave simulation is shown in Fig. 9. To avoid the intersection of microstrip lines at some points, e.g., one path connecting to port 3, signals need to be transitioned from the bottom layer to top layer using metallic via, and then transitioned back to the bottom layer. It is noted that the order of the output port is not from port 7 to port 12, which is due to the intrinsic phase distribution of the network.

Fig. 10 shows the full-wave simulation result of the 6 × 6 BFN. All of the transmission coefficients from input ports to output ports $|S_{ij}|$ (i = 1, 2, .., 6, j = 7, 8, …, 12) are displayed in Fig. 11(a). It is observed that the simulated $|S_{ij}|$ is ranged from -10.2 dB to -7.8 dB in the band of 3.2-4.8 GHz. The return

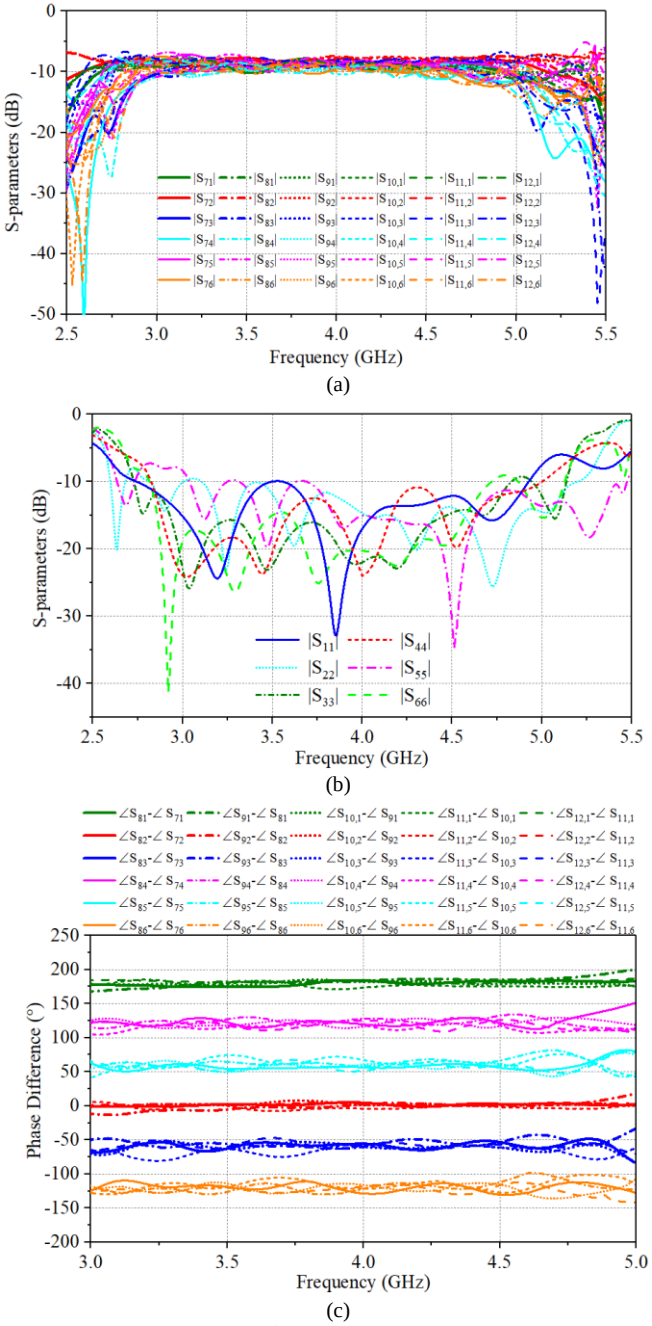

Fig. 10. Simulation results of the 5-beam 6 × 6 BFN: (a) transmission coefficients; (b) reflection coefficients; (c) phase difference.

loss is below -10 dB. Six different phase intervals, i.e., -180°, 0°, -60°, 120°, 60° and -120°, are realized, and the phase deviation is about ±9°.

Using the same design method, it is possible to layout the modified 6 × 6 BFN given in Fig. 1(b). In comparison to the 5-beam case, the 6-beam one uses more phase shifters. Since the -60° phase shifters are connected to the first output of the 3 × 3 BFN, it is possible to combine it with the 90° phase shifter and merge the phase shift value to 30°. The layout structure is displayed in Fig. 11. Some delay lines are used to compensate the phase introduced by the phase shifters. The S-parameters of the 6-beam BFN are very similar to the 5-beam one, and thus are not shown here for simplicity. Fig. 12 shows the simulation

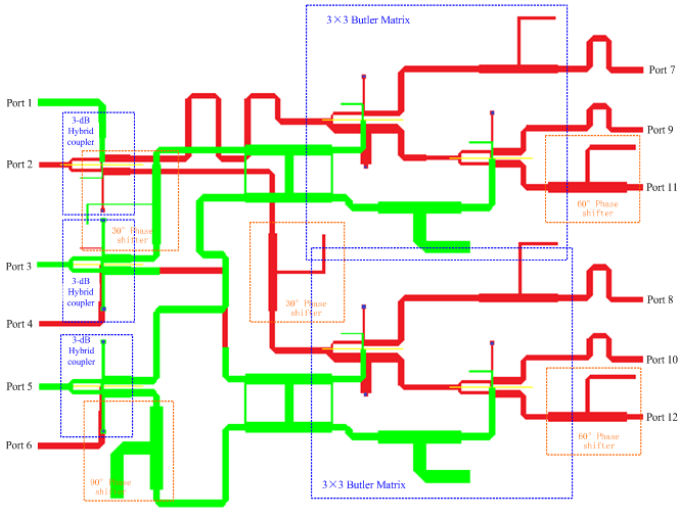

Fig. 11. Layout of the modified 6-beam BFN.

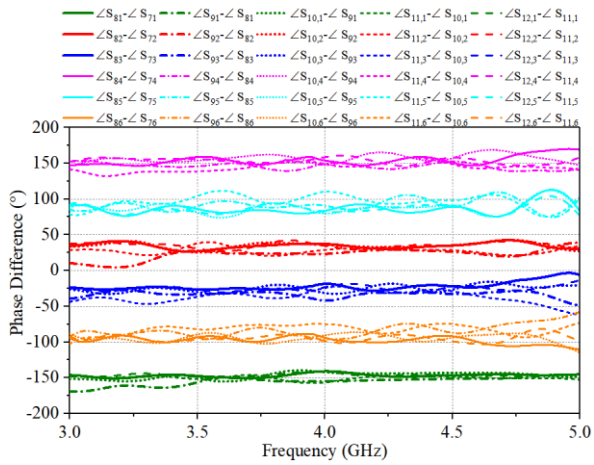

Fig. 12. Simulated phase difference of the modified 6-beam BFN.

result of the phase difference between any two adjacent ports. The phase intervals for port 1 to port 6 are -150°, 30°, -150°, 150°, 90° and -90°, respectively, which are in line with the predicted values from analysis. The phase deviation is about ±12°, which is a little bit larger than the 5-beam case.

B. Measurement of the 5-beam BFN and Array Patterns

For verification purpose, the 5-beam BFN is fabricated, and based on which, experiments have been conducted. The fabricated prototype is shown in Fig. 13. It is tested using Vector Network Analyzer. All the S-parameters and phase performance are displayed in Fig. 14. The measured transmission coefficients $|S_{ij}|$ (i = 1, 2, .., 6, j = 7, 8, …, 12) are ranged from -11.6 dB to -8.5 dB, indicating that the insertion loss is around 0.7 to 3.8 dB. For the return loss, the measured 10-dB matching band is from 2.9 to 4.7 GHz (bandwidth is 47.4%). It is observed that the measured results agree with the simulated ones very well. Both the simulation and the tested results reveal that this design has a wide operating bandwidth. If taking both of the magnitude and phase into consideration, the operating band range is from 3.12 to 4.65 GHz, and the fractional bandwidth is around 39.4%, which exceeds all the existing BFNs with similar functions.

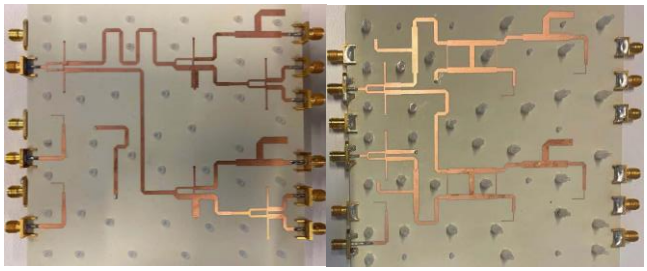

(a) (b)

Fig. 13. Fabricated prototype of the 5-beam 6 × 6 BFN: (a) front-side view; (b) back-side view.

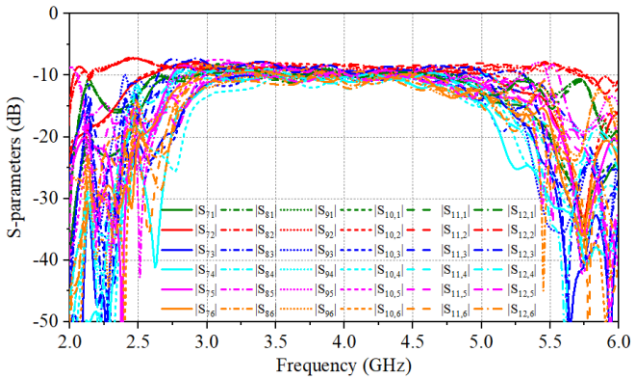

(a)

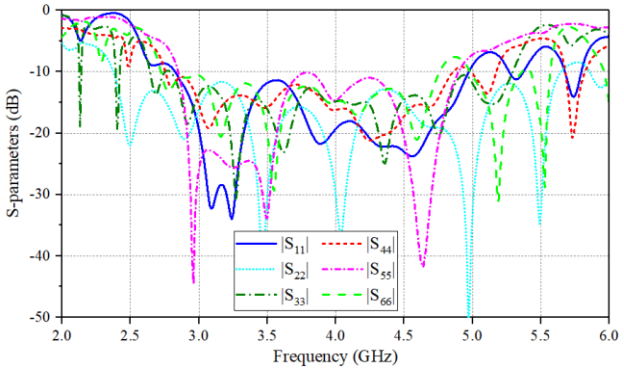

(b)

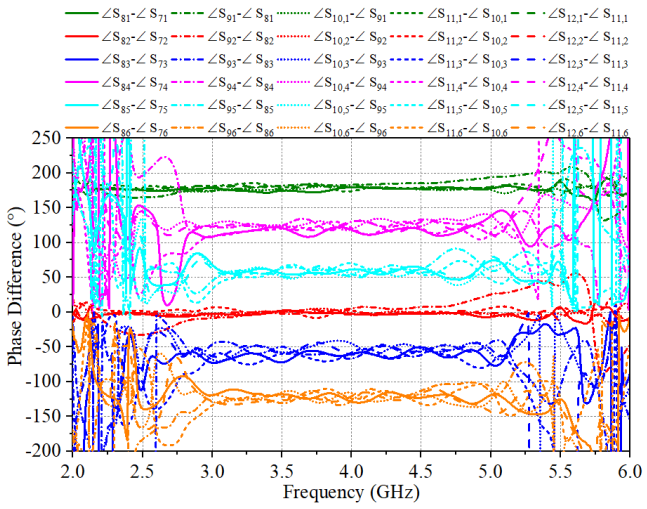

(c)

Fig. 14. Measured results of the fabricated 5-beam BFN: (a) transmission coefficients; (b) reflection coefficients; (c) phase difference.

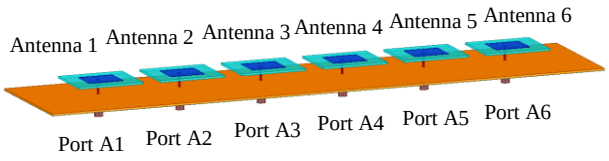

Fig. 15. Antenna array fed by the proposed BFN.

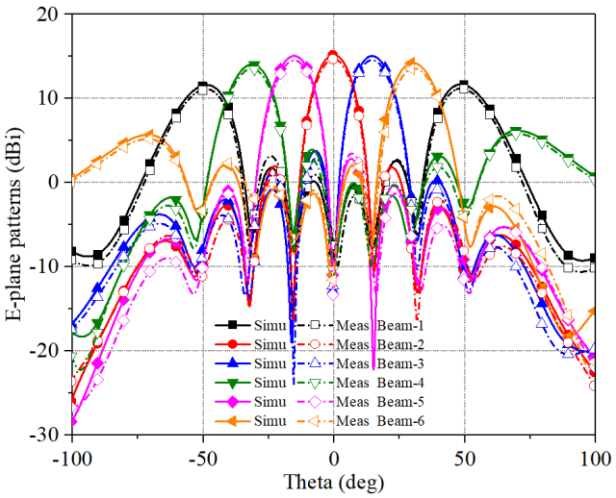

Fig. 16. E-plane patterns on the antenna array at 4 GHz when fed by the proposed 5-beam 6 × 6 BFN.

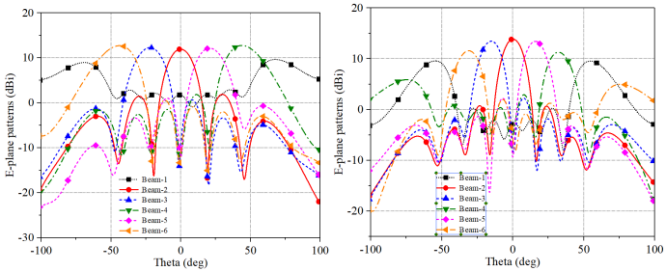

(a) (b)

Fig. 17. E-plane patterns of the 5-beam array at: (a)3.5 GHz; (b) 4.5 GHz.

Since the 5-beam 6 × 6 BFN is tested and verified, the 6-beam 6 × 6 BFN is not tested due to the fact that the same procedure is used compared with the 5-beam one. To demonstrate the function of the proposed beam-forming networks, we use the proposed 6 × 6 BFN to feed a 6-element linear array displayed in Fig. 15. The purpose is to produce similar patterns as predicted in Fig. 3. Since the proposed beamforming network has a wide operating bandwidth, the antenna array should have 30% wideband as well. The substrate of the antenna array is FR4 with dielectric constant of 4.4 and thickness of 1 mm.

A rectangular patch antenna is printed on a smaller substrate which is hanged in the air using nylon posts to support it. Another substrate with larger size is used below the upper substrate, where the ground plane is printed on the backside. For each element, the length and width of the patch antenna are equal to 21.6 mm. There are four circular patches with the radius of 1 mm printed on the backside of the substrate, and the position of the circular patch is located at the upper positions of four feeding points of the patch antenna. The inner conductors of four feeding cables would be connected with these four

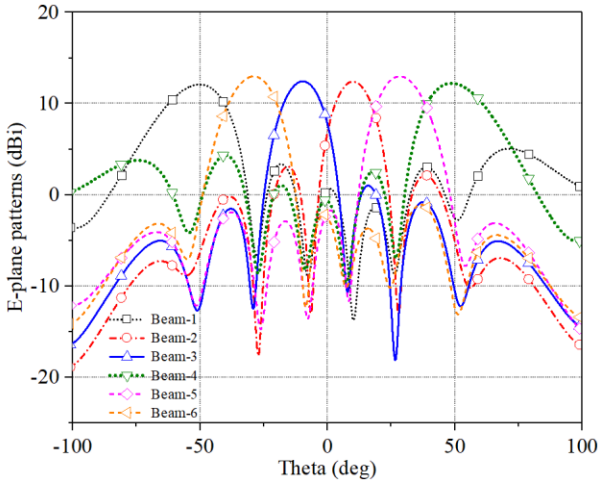

Fig. 18. E-plane patterns of the modified 6-beam array at 4 GHz.

circular patches, to excite the rectangular patch antenna. The lengths of the upper and lower substrate are 38 mm and 80 mm, respectively. The distance between the upper and lower substrates is 7 mm, and the distance between two non-adjacent feed points is 13.4 mm. The inner conductor of the feeding cable is extended via an air hole through ground and the lower substrate, and then connected to the circular patch on the bottom layer of the upper substrate, while the outer conductor is connected with the ground. The spacing between adjacent elements is 42 mm.

Pattern evaluation has been done in full-wave environment using the excitations provided by the proposed BFNs from EM simulation and measurement. The input ports of antennas labeled A1 to A6 should be connected to port 7 to 12 of the beamforming network, respectively. Fig. 16 depicts the E-plane patterns at the center frequency 4 GHz in simulation and measurement, where one can observe that five different patterns and a differential pattern are realized. The boresight beam has a high gain value of 15.2 dBi, and it varies to 14.6 dBi and 13.8 dBi when the beams radiate towards to ±15° and ±31°, respectively. The remaining beam has a differential pattern with two maximum gain points at –48° and 48°, which is also in line with prediction.

To illustrate the wideband performance of the beamforming networks, the radiation patterns at 3.5 GHz and 4.5 GHz are given in Fig. 17. It is obvious that multiple beams can be produced at the edge frequencies, indicating wideband performance of the antenna array fed by the proposed BFN. Simulated E-plane radiation patterns of the antenna array fed by the modified 6-beam BFN are also given in Fig. 18. All the above- mentioned radiation patterns demonstrate the beam-forming capability of the proposed BFNs.

V. Extended Higher-Order 12 × 12 Beamforming Network

Based on the proposed 6 × 6 BFN, it is also possible to extend the proposed 6 × 6 BFN to higher orders, such as a 12 × 12 BFN which can produce 12 beams. This 12 × 12 BFN combines the functions of the 5-beam and modified 6-beam BFN in one network. Its configuration is displayed in Fig. 18. The core components of the 12 × 12 network are the same with

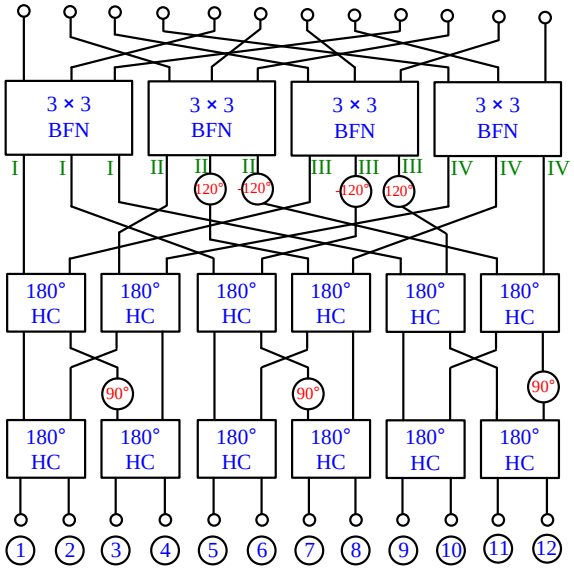

Fig. 19. The configuration of a 12 × 12 BFN.

Table II Phase Distribution and Phase Increment

Port/ Angles	I	II	III	IV	$\Delta\varphi$
①	0º	0º	0º	0º	0º
②	0º	180º	0º	180º	180º
③	90º	0º	-90º	-180º	-90º
④	90º	180º	-90º	0º	90º
⑤	0º	120º	-120º	0º	120º
⑥	0º	-60º	-120º	-180º	-60º
⑦	90º	120º	150º	180º	30º
⑧	90º	-60º	150º	0º	-150º
⑨	0º	-120º	120º	0º	-120º
⑩	0º	60º	120º	180º	60º
⑪	0º	-30º	-60º	-120º	-30º
⑫	0º	150º	-60º	90º	150º

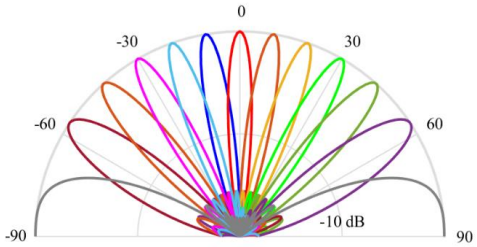

Fig. 20. Radiation patterns produced by a 12-beam BFN.

the 6 × 6 one, which are 3 × 3 BFNs and 180º hybrid couplers. The key idea is to excite four 3 × 3 BFNs to produce 12 output signals with equal magnitude and identical phase increment. To this end, one needs to use two rows of hybrid couplers, where each row comprises 6 hybrid couplers, all together 12 couplers. These couplers can be divided to three groups, and each group has four couplers, two on each row. Each group of couplers has four output signals, which are the input signals of four 3 × 3 BFNs and referred to as the positions of I, II, III and IV in the figure. To produce 12 different beams, the output phase of each coupler group should be different, considering the fact that when the 3 × 3 BFN can produce three phase increments of 0°. To this end, three 90° phase shifters are used between two rows of hybrid couplers. Another four phase shifters with 120º and -120º phase shift are also needed to guarantee the phase increment at the output ports.

The phase distribution at the positions of I, II, III and IV and the phase increment of each port are listed in Table II. It is found that 12 different kinds of phase increment are realized from -180º to 180º with 30º interval. Using this 12 × 12 BFN, one can connect it with a 12-element linear array to produce 12 beams including one at the boresight and one differential beam. Fig. 19 depicts the radiation patterns of these beams, which have exactly the same beam angles, narrower beam-width and higher gain compared with those presented in Figs. 3 and 4. This demonstrates that the extended 12 × 12 BFN can realize the functions of the proposed 5-beam and modified 6-beam BFN in one network. This network can be used as a 12-beam network, which provides more flexibility in choosing beam numbers in multi-beam applications.

VI. Conclusion

This paper proposed two designs of wideband 6 × 6 BFNs, which can produce 5 and 6 orthogonal beams in a 1-D plane. The designs are analyzed and synthesized first, and then are verified in electromagnetic implementation using planar structures. Since wide bandwidth is aimed, a wideband 180° hybrid coupler is firstly developed, followed by a 3 × 3 BFN design. Based on these two designs and phase shifters, 5- and 6-beam BFNs are realized, and both designs have more than 35% operating bandwidth. Finally, a linear array is fed by a fabricated prototype, and multiple patterns are realized as expected successfully, demonstrating the beam- forming function of the proposed multi-beam networks.

References

[1] Y. J. Guo and R.W. Ziolkowsk, *Advanced Antenna Array Engineering for 6G and Beyond Wireless Communications*. Hoboken, NJ, USA: Wiley, 2021.

[2] W. Hong et al., "Multi-beam antenna technologies for 5G wireless communications," *IEEE Trans. Antennas Propag*., vol. 65, no. 12, pp. 6231–6249, Dec. 2017

[3] J.-W. Lian, Y.-L. Ban, H. Zhu, and Y. J. Guo, "Uniplanar beam-forming network employing eight-port hybrid couplers and crossovers for 2-D multi-beam array antennas," *IEEE Trans. Microw. Theory Techn*., vol. 68, no. 11, pp. 4706–4718, Nov. 2020.

[4] N. J. G. Fonseca, "Design and implementation of a closed cylindrical BFN-fed circular array antenna for multiple-beam coverage in azimuth," *IEEE Trans. Antennas Propag*., vol. 60, no. 2, pp. 863–869, Feb. 2012

[5] J. Blass, "Multidirectional antenna-a new approach to stacked beams," in 1958 IRE International Convention Record, vol. 8. IEEE, 1966, pp. 48–50.

[6] S. Mosca, F. Bilotti, A. Toscano, and L. Vegni, "A novel design method for Blass matrix beam-forming networks," *IEEE Trans. Antennas Propag*., vol. 50, no. 2, pp. 225–232, Feb. 2002.

[7] Butler, J.; Lowe, R., "Beam forming matrix simplifiers design of electrically scanned antennas", *Electronic Design*, 1961.

[8] M. Ansari, H. Zhu, N. Shariati, and Y. J. Guo, "Compact planar beam-forming array with end-fire radiating elements for 5G applications," *IEEE Trans. Antennas Propag*., vol. 67, no. 11, pp. 6859–6869, Nov. 2019.

[9] J. Nolen, "Synthesis of multiple beam networks for arbitrary illuminations," Ph.D. dissertation, Bendix Corp., Radio Div., Baltimore, MD, Apr. 1965.

[10] N. J. G. Fonseca, "Printed S-band 4 × 4 Nolen matrix for multiple beam antenna applications," *IEEE Trans. Antennas Propag*., vol. 57, no. 6, pp. 1673–1678, Jun. 2009.

[11] H. Ren, H. Zhang, Y. Jin, Y. Gu and B. Arigong, "A Novel 2-D 3×3 Nolen Matrix for 2-D Beamforming Applications," in *IEEE Trans. Microw. Theory Techn*., vol. 67, no. 11, pp. 4622-4631, Nov. 2019.

[12] M. Ansari, B. Jones, H. Zhu, N. Shariati, and Y. J. Guo, "A highly efficient spherical Luneburg lens for low microwave frequencies realized with a metal-based artificial medium," *IEEE Trans. Antennas Propag*., vol. 69, no. 7, pp. 3758–3770, Jul., 2021.

[13] J.-W. Lian, Y.-L. Ban, H. Zhu, and Y. Guo, "Reduced-sidelobe multi-beam array antenna based on SIW Rotman lens," *IEEE Antennas Wireless Propag. Lett.*, vol. 29, no. 1, pp. 188–192, Dec. 2019.

[14] A. Tajik, A. Alavijeh, and M. Fakharzadeh, "Asymmetrical 4 × 4 Butler matrix and its application for single layer 8 × 8 Butler matrix," *IEEE Trans. Antennas Propag*., vol. 67, no. 8, pp. 5372–5379, Aug. 2019.

[15] H. Zhu, P. Qin, and Y. J. Guo, "Single-ended-to-balanced power divider with extended common-mode suppression and its application to differential 2 × 4 Butler matrices," *IEEE Trans. Microw. Theory Techn*., vol. 68, no. 4, pp. 1510–1519, Apr. 2020.

[16] J. W. Lian, Y. L. Ban, Q. L. Yang, B. Fu, Z. F. Yu and L. K. Sun, "Planar millimeter-wave 2-D beam-scanning multibeam array antenna fed by compact SIW beam-forming network" *IEEE Trans. Antennas Propag*., vol. 66, no. 3, pp. 1299–1310, Mar. 2018.

[17] K. Tekkouk, J. Hirokawa, R. Sauleau, M. Ettorre, M. Sano, and M. Ando, "Dual-layer ridged waveguide slot array fed by a Butler matrix with sidelobe control in the 60-GHz band," *IEEE Trans. Antennas Propag*., vol. 63, no. 9, pp. 3857–3867, Sep. 2015.

[18] L. G. Sodin, "Method of synthesizing a beam-forming device for the N-beam and N-element array antenna, for any N," *IEEE Trans. Antennas Propag*., vol. 60, no. 4, pp. 1771–1776, Apr. 2012.

[19] T. Djerafi, N. J. G. Fonseca and K. Wu, "Planar Ku-band 4×4 Nolen matrix in SIW technology," in *IEEE Transactions on Microwave Theory and Techniques*, vol. 58, no. 2, pp. 259-266, Feb. 2010.

[20] N. J. G. Fonseca and N. Ferrando, "Nolen matrix with tapered amplitude law for linear arrays with reduced side lobe level," in *Proc. 4th Eur. Conf. Antennas Propag.*, Barcelona, Spain, 2010, pp. 1–5.

[21] T. Djerafi, N. J. G. Fonseca and K. Wu, "Broadband substrate integrated waveguide 4×4 Nolen matrix based on coupler delay compensation," in *IEEE Trans. Microw. Theory Techn*, vol. 59, no. 7, pp. 1740-1745, July 2011.

[22] J. Hirokawa and N. J. G. Fonseca, "Generalized one-dimensional parallel switching matrices with an arbitrary number of beams," in *IEEE J. Microw.*, vol. 1, no. 4, pp. 975-988, Oct. 2021.

[23] J. Hirokawa, and N. J. G. Fonseca, "One-body two-dimensional switching matrices with a triangular lattice of beams," *IEEE Antennas Wireless Propag. Lett*, vol. 21, no. 3, pp. 581-585, 2022.

[24] J. P. Shelton and K. S. Kelleher, "Multiple beams from linear arrays," *IRE Trans. Antennas Propag*., vol. 9, pp. 154–161, Mar. 1961.

[25] A. Angelucci, P. Audagnotto, P. Corda, and B. Piovano, "Multiport power amplifiers for mobile-radio systems using microstrip Butler matrices," in *Int. Symp. Antennas Propag. (AP-S), Dig.*, vol. 1. 1994, pp. 628–631.

[26] B. Piovano et al., "Design and breadboarding of wideband Butler matrices for multiport amplifiers," in *Proc. SBMO Int Microw. Conf*., Brazil, August 2–5, 1993, pp. 175–180.

[27] S. Odrobina, K. Staszek, K. Wincza, and S. Gruszczynski, "Broadband 3 × 3 Butler matrix," in *Proc. Conf. Microw. Techn. (COMITE)*, Apr. 2017, pp. 1–5.

[28] J. P. Wang, S.-H. Hsu, and W.-J. Chen, "Two-Layer three-beam generating matrix for broadband beamforming with microstrip," in *Proc. IEEE Int. Symp. Antennas Propag*. (AP-S), Jul. 2017, p. 2347.

[29] H. Zhu, H. Sun, B. Jones, C. Ding, and Y. J. Guo, "Wideband dual-polarized multiple beam-forming antenna arrays," *IEEE Trans. Antennas Propag.*, vol. 67, no. 3, pp. 1590–1604, Mar. 2019.

[30] M. Traii, A. Gharsallah, " Mutual Coupling in Phased Arrays For 3x4 Butler Matrices Antenna Network", *IEEE International Conference on Signals, Circuits and Systems, (SCS'08),* Tunisia, Nov. 2008.

[31] H. Nachouane *et al*., "Wideband 3 × 4 Butler matrix using Wilkinson divider for MIMO applications," in *Proc. Int. Conf. Next Gener. Netw. Serv*., 2014, pp. 101–105.

[32] K. Xiang, F. Chen, Q. Chu, and M. J. Lancaster, "A broadband 3 × 4 Butler matrix and its application in multibeam antenna arrays," *IEEE Trans. Antennas Propag.*, vol. 67, no. 12, pp. 7622–7627, Dec. 2019.

[33] C. Qin, F. –C. Chen, and K. –R. Xiang, "A 5 × 8 Butler matrix based on substrate integrated waveguide technology for millimeter-wave multibeam application," *IEEE Antennas Wireless Propag. Lett*., vol. 20, no. 7, pp. 1292–1296, Jul. 2014.

[34] R. J. Gong, Y. L. Ban, J. W. Lian, Y. Liu, and Z. Nie, "Circularly polarized multibeam antenna array of ME dipole fed by 5× 6 Butler matrix," *IEEE Antennas Wireless Propag. Lett*., vol. 18, no. 4, pp. 712–716, Apr. 2019.

[35] Y. Yang, Y. -L. Ban, Q. Yang, J. -W. Lian, Q. Sun, and G. Wu, "Millimeter wave wide-angle scanning circularly polarized antenna array with a novel polarizer", *IEEE Trans. Antennas Propag*., vol. 70, no.2, pp. 1077–1086, Feb. 2022.

[36] K. Ding, J. Bai, and A. Kishk, "A quasi Butler matrix with 6×6 beamforming capacity using 3×3 hybrid couplers," in *Proc. 32nd Gen. Assem. Sci. Symp. Int. Union Radio Sci.*, Montreal, QC, Canada, Aug. 2017, pp. 1–4.

[37] H. Zhu, T. Zhang and Y. J. Guo, "Wideband hybrid couplers with unequal power division/arbitrary output phases and applications to miniaturized Nolen matrices," in *IEEE Transactions on Microwave Theory and Techniques*, early access, doi: 10.1109/TMTT.2022.3164673.

[38] H. Zhu, Z. Cheng, and Y. J. Guo, "Design of wideband in-phase and out-of-phase power dividers using microstrip-to-slotline transitions and slotline resonators," *IEEE Trans. Microw. Theory Techn.*, vol. 67, no. 4, pp. 1412–1424, Apr. 2019.

[39] K. C. Gupta, R. Garg, I. Bahl, and P. Bhartia, *Microstrip Lines and Slotlines*, 2nd ed. Norwood, MA, USA: Artech House, 1996.